Microscopic analysis of sub-barrier fusion enhancement in ^{132}Sn+^{40}Ca versus ^{132}Sn+^{48}Ca

V. E. Oberacker and A. S. Umar

Phys. Rev. C **87**, 034611 — Published 7 March 2013

DOI: 10.1103/PhysRevC.87.034611

Microscopic analysis of sub-barrier fusion enhancement in ^{132}Sn+^{40}Ca vs. ^{132}Sn+^{48}Ca

V.E. Oberacker[1] and A.S. Umar[1]

[1] *Department of Physics and Astronomy, Vanderbilt University, Nashville, Tennessee 37235, USA*

(Dated: February 7, 2013)

We provide a theoretical analysis of recently measured fusion cross sections which show a surprising enhancement at low $E_{\rm c.m.}$ energies for the system ^{132}Sn+^{40}Ca as compared to the more neutron-rich system ^{132}Sn+^{48}Ca. Dynamic microscopic calculations are carried out on a three-dimensional lattice with a time-dependent density-constrained density functional theory. There are no adjustable parameters, the only input is the Skyrme effective NN interaction. Heavy-ion potentials $V(R)$, coordinate-dependent mass parameters $M(R)$, and total fusion cross sections $\sigma(E_{\rm c.m.})$ are calculated for both systems. We are able to explain the measured fusion enhancement in terms of the *narrower width* of the ion-ion potential for ^{132}Sn+^{40}Ca, while the barrier heights and positions are approximately the same in both systems.

PACS numbers: 21.60.-n,21.60.Jz

I. INTRODUCTION

Radioactive ion beam facilities enable us to study fusion reactions with exotic neutron-rich nuclei. An important goal of these experiments is to study the effects of neutron excess $(N-Z)$ on fusion. In several experiments, large enhancements of sub-barrier fusion yields have been observed for systems with positive Q values for neutron transfer. Recently, at the HRIBF facility a series of experiments has been carried out with radioactive ^{132}Sn beams and with stable ^{124}Sn beams on ^{40,48}Ca targets [1]. It turns out that the ^{40}Ca+Sn systems have many positive Q values for neutron-pickup while all the Q values for ^{48}Ca+Sn are negative. However, the data analysis reveals that the fusion enhancement is not proportional to the magnitudes of those Q values.

Particularly puzzling is the experimental observation of a sub-barrier fusion enhancement in the system ^{132}Sn+^{40}Ca as compared to more neutron-rich system ^{132}Sn+^{48}Ca. This is difficult to understand because the 8 additional neutrons in ^{48}Ca should increase the attractive strong nuclear interaction and thus lower the fusion barrier, resulting in an enhanced sub-barrier fusion cross section. But the opposite is found experimentally. A coupled channel analysis [1] of the fusion data with phenomenological heavy-ion potentials yields cross sections that are one order of magnitude too small at sub-barrier energies, despite the fact that these ion-ion potentials contain many adjustable parameters.

The time-dependent Hartree-Fock (TDHF) theory provides a useful foundation for a fully microscopic many-body theory of large amplitude collective motion [2, 3] including deep-inelastic and fusion reactions. But only in recent years has it become feasible to perform TDHF calculations on a 3D Cartesian grid without any symmetry restrictions and with much more accurate numerical methods [3–8]. In addition, the quality of effective interactions has been substantially improved [9–12]. During the past several years, we have developed the Density Constrained Time-Dependent Hartree-Fock (DC-TDHF) method for calculating heavy-ion potentials [13], and we have applied this method to calculate fusion and capture cross sections above and below the barrier. As of to date, we have studied a total of 18 different systems, including ^{132,124}Sn+^{96}Zr [14], ^{132}Sn+^{64}Ni [15, 16], ^{16}O+^{208}Pb [17], and hot and cold fusion reactions leading to superheavy element $Z = 112$ [18]. Most recently, we have investigated sub-barrier fusion and pre-equilibrium giant resonance excitation between various calcium + calcium isotopes [19], and between isotopes of oxygen and carbon [20] that occur in the neutron star crust. In all cases, we have found good agreement between the measured fusion cross sections and the DC-TDHF results. This is rather remarkable given the fact that the only input in DC-TDHF is the Skyrme effective N-N interaction, and there are no adjustable parameters.

This paper is organized as follows: in Section II we summarize the theoretical formalism and show results for the ion-ion potentials calculated with the DC-TDHF method. In Section III, we discuss the corresponding total fusion cross sections, and we explain the observed fusion enhancement in terms of the *narrower width* of the ion-ion potential for ^{132}Sn+^{40}Ca. Our conclusions are presented in Section IV.

II. THEORETICAL FORMALISM AND ION-ION POTENTIALS

Currently, a true quantum many-body theory of barrier tunneling does not exist. All sub-barrier fusion calculations assume that there exists an ion-ion potential $V(R)$ which depends on the internuclear distance R. Most of the theoretical fusion studies are carried out with the coupled-channels (CC) method [21–24] in which one uses empirical ion-ion potentials (typically Woods-Saxon potentials, or double-folding potentials with frozen nuclear densities).

While phenomenological methods provide a useful starting point for the analysis of fusion data, it is desirable to use a quantum many-body approach which properly describes the underlying nuclear shell structure

of the reaction system. We have developed a microscopic approach to extract heavy-ion interaction potentials $V(R)$ from the TDHF time-evolution of the dinuclear system. The interaction potentials calculated with the DC-TDHF method incorporate all of the dynamical entrance channel effects such as neck formation, particle exchange, internal excitations, and deformation effects [25]. While the outer part of the potential barrier is largely determined by the entrance channel properties, the inner part of the potential barrier is strongly sensitive to dynamical effects such as particle transfer and neck formation.

The TDHF equations for the single-particle wave functions

$$h(\{\phi_\mu\})\ \phi_\lambda(r,t) = i\hbar\frac{\partial}{\partial t}\phi_\lambda(r,t) \quad (\lambda = 1, ..., A)\ , \quad (1)$$

can be derived from a variational principle. The main approximation in TDHF is that the many-body wave function $\Phi(t)$ is assumed to be a single time-dependent Slater determinant which consists of an anti-symmetrized product of single-particle wave functions

$$\Phi(r_1, ..., r_A; t) = (A!)^{-1/2}\ det|\phi_\lambda(r_i, t)|\ . \quad (2)$$

In the present TDHF calculations we use the Skyrme SLy4 interaction [9] for the nucleons including all of the time-odd terms in the mean-field Hamiltonian [5]. The numerical calculations are carried out on a 3D Cartesian lattice. For ^{40,48}Ca+^{132}Sn the lattice spans 50 fm along the collision axis and $30-42$ fm in the other two directions, depending on the impact parameter. First we generate very accurate static HF wave functions for the two nuclei on the 3D grid. In the second step, we apply a boost operator to the single-particle wave functions. The time-propagation is carried out using a Taylor series expansion (up to orders $10-12$) of the unitary mean-field propagator, with a time step $\Delta t = 0.4$ fm/c.

In our DC-TDHF approach, the time-evolution takes place with no restrictions. At certain times t or, equivalently, at certain internuclear distances $R(t)$ the instantaneous TDHF density

$$\rho_{\rm TDHF}(r,t) =< \Phi(t)|\rho|\Phi(t) > \quad (3)$$

is used to perform a static Hartree-Fock energy minimization

$$\delta < \Phi_\rho\ |H - \int d^3r\ \lambda(r)\ \rho(r)\ |\Phi_\rho >= 0 \quad (4)$$

while constraining the proton and neutron densities to be equal to the instantaneous TDHF densities

$$< \Phi_\rho|\rho|\Phi_\rho >= \rho_{\rm TDHF}(r,t)\ . \quad (5)$$

These equations determine the state vector Φ_ρ. This means we allow the single-particle wave functions to rearrange themselves in such a way that the total energy is minimized, subject to the TDHF density constraint.

In a typical DC-TDHF run, we utilize a few thousand time steps, and the density constraint is applied every $10-20$ time steps. We refer to the minimized energy as the "density constrained energy" $E_{\rm DC}(R)$

$$E_{\rm DC}(R) =< \Phi_\rho|H|\Phi_\rho >\ . \quad (6)$$

The ion-ion interaction potential $V(R)$ is essentially the same as $E_{\rm DC}(R)$, except that it is renormalized by subtracting the constant binding energies $E_{\rm A_1}$ and $E_{\rm A_2}$ of the two individual nuclei

$$V(R) = E_{\rm DC}(R) - E_{\rm A_1} - E_{\rm A_2}\ . \quad (7)$$

In Fig. 1 we compare the heavy-ion interaction potentials $V(R)$ for the systems ^{132}Sn+^{40,48}Ca. It should be noted that DC-TDHF contains particle transfer "on average" [19], but it does not describe individual transfer channels. We find the unexpected result that the barrier heights and positions are approximately the same in both cases, but the *barrier width* for ^{132}Sn+^{40}Ca is substantially smaller.

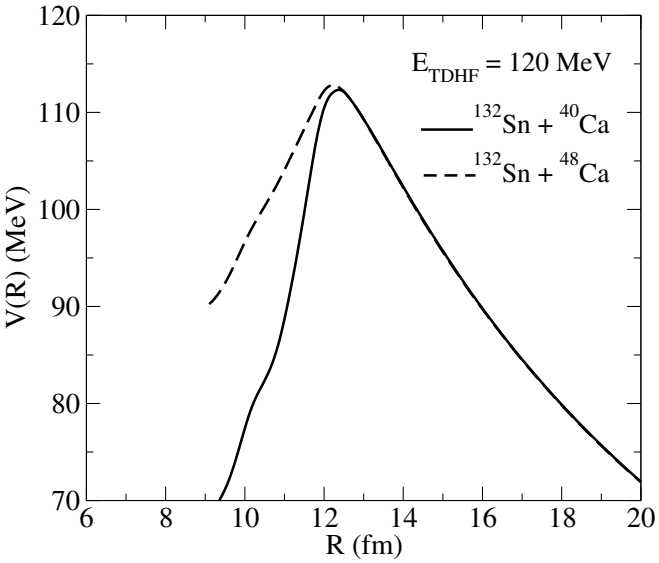

FIG. 1. DC-TDHF calculation of the heavy-ion potentials $V(R)$ for the systems ^{132}Sn+^{40,48}Ca. The ion-ion potentials are energy-dependent and have been calculated at $E_{\rm TDHF} =$ 120 MeV.

Using TDHF dynamics, it is also possible to compute the corresponding coordinate dependent mass parameter $M(R)$ [17]. At large distance R, the mass $M(R)$ is equal to the reduced mass μ of the system. At smaller distances, when the nuclei overlap, the mass parameter generally increases. We find that the structure of $M(R)$ for the ^{132}Sn+^{40}Ca reaction is fairly similar to the mass parameter calculated for ^{132}Sn+^{48}Ca (see Fig. 6 of Ref. [26]), and it is therefore not shown here.

Instead of solving the Schrödinger equation with coordinate dependent mass parameter $M(R)$ for the heavy-ion potential $V(R)$, it is numerically advantageous to

use the constant reduced mass μ and to transfer the coordinate-dependence of the mass to a scaled potential $U(\bar{R})$ using a scale transformation

$$(R, M(R), V(R)) \longrightarrow (\bar{R}, \mu, U(\bar{R})) \ . \qquad (8)$$

Details are given in Ref. [17]. In order to calculate the fusion cross section, one can either use the coordinate-dependent mass $M(R)$ and the original potential $V(R)$ or, equivalently, the constant mass μ and the transformed potential $U(\bar{R})$. The latter is advantageous for numerical reasons. As a result of the scale transformation to constant mass μ, the potential barriers $U(\bar{R})$ for *both* systems ^{132}Sn+^{40,48}Ca are broadened in the interior region (see Fig. 2) as compared to the original potentials $V(R)$ in Fig. 1.

In Fig. 2 we display the transformed potentials $U(\bar{R})$ which correspond to the constant reduced mass μ. A comparison of Fig. 1 and Fig. 2 reveals that the coordinate-dependent mass changes only the interior region of the potential barriers, and this change is most pronounced at low $E_{\rm c.m.}$ energies. Note that the transformation to a constant mass parameter preserves the basic features found for the original potentials, i.e. the *narrower width* of the ion-ion potential for ^{132}Sn+^{40}Ca, while the barrier heights and positions are approximately the same in both systems.

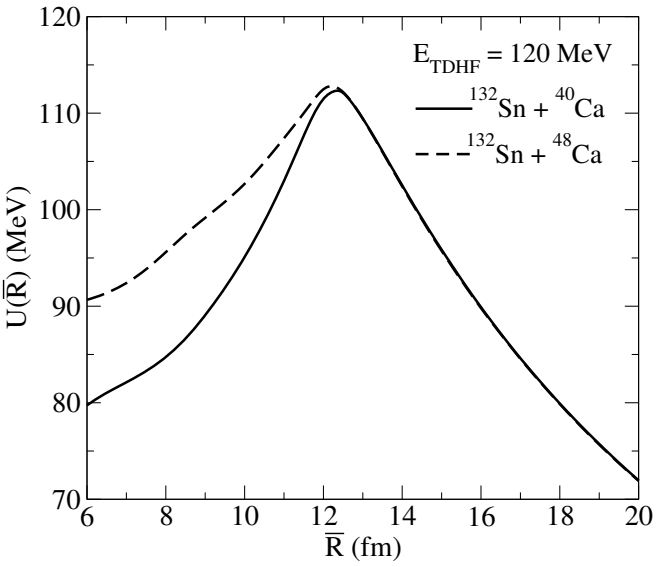

FIG. 2. Transformed heavy-ion potentials $U(\bar{R})$ corresponding to the constant reduced mass μ.

In general, our DC-TDHF calculations show that *ion-ion potentials for heavy systems are strongly energy-dependent*. By contrast, DC-TDHF calculations for light ion systems such as ^{16}O+^{16}O show almost no energy-dependence even if we increase $E_{\rm c.m.}$ by a factor of four [27]. Even in reactions between a light and a very heavy nucleus such as ^{16}O+^{208}Pb, we see only a relatively weak energy dependence of the barrier height and width [17]. In Fig. 3 the original potentials $V(R)$ (solid lines) and the transformed potentials $U(\bar{R})$ are shown at three different TDHF energies. We use the label $E_{\rm TDHF}$ to indicate the TDHF center-of-mass energy for which the ion-ion potential $V(R)$ has been calculated. Once $V(R)$ has been obtained, it can, in principle, be used to calculate the fusion cross section for all $E_{\rm c.m.}$ energies (see e.g. Fig. 4). Of course, if the potentials are found to be strongly energy-dependent, they should be applied for $E_{\rm c.m.}$ intervals in the vicinity of a given $E_{\rm TDHF}$. We notice that in these heavy systems the potential barrier height increases dramatically with increasing energy $E_{\rm TDHF}$, and the barrier peak moves inward towards smaller internuclear distances. The potential $U(\bar{R})$ calculated at high energy ($E_{\rm TDHF} = 180$ MeV) has a barrier $E_B = 115.3$ MeV located at $\bar{R} = 11.8$ fm, whereas the potential calculated at low energy ($E_{\rm TDHF} = 120$ MeV) has a barrier of only $E_B = 112.3$ MeV located at $\bar{R} = 12.4$ fm.

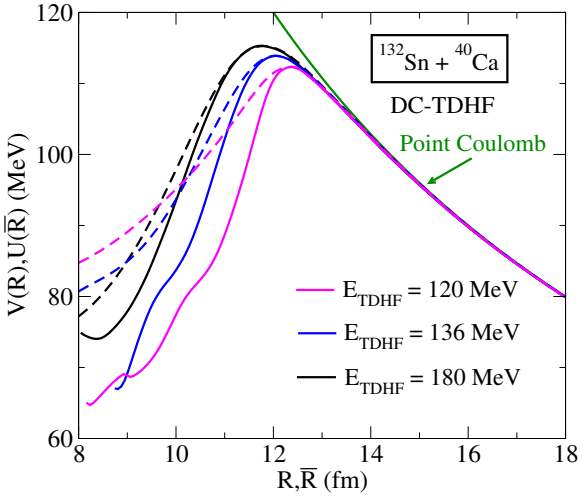

FIG. 3. (Color online) Solid lines: original heavy-ion potentials $V(R)$. Dashed lines: transformed potentials $U(\bar{R})$ corresponding to the reduced mass μ. The potentials have been calculated at three different energies.

The Schrödinger equation corresponding to the constant reduced mass μ and the scaled potential $U(\bar{R})$ has the familiar form

$$\left[\frac{-\hbar^2}{2\mu}\frac{d^2}{d\bar{R}^2} + \frac{\hbar^2\ell(\ell+1)}{2\mu\bar{R}^2} + U(\bar{R}) - E_{\rm c.m.}\right]\psi_\ell(\bar{R}) = 0 \ . \qquad (9)$$

By numerical integration of Eq. (9) using the well-established *Incoming Wave Boundary Condition* (IWBC) method [21] we obtain the barrier penetrabilities T_ℓ which determine the total fusion cross section

$$\sigma_{\rm fus}(E_{\rm c.m.}) = \frac{\pi\hbar^2}{2\mu E_{\rm c.m.}}\sum_{\ell=0}^{\infty}(2\ell+1)T_\ell(E_{\rm c.m.}) \ . \qquad (10)$$

III. FUSION CROSS SECTIONS

In Figures 4 and 5 we show fusion cross sections measured at HRIBF [1] for the systems ^{132}Sn+^{40,48}Ca. A comparison of the fusion cross sections at low energies yields the surprising result that fusion of ^{132}Sn with ^{40}Ca yields a larger cross section than with ^{48}Ca. For example, at $E_{\rm c.m.} = 110$ MeV we find an experimental cross section of ≈ 6 mb for ^{132}Sn+^{40}Ca as compared to 0.8 mb for the more neutron-rich system ^{132}Sn+^{48}Ca. If the data are scaled for trivial size effects (nuclear radii) the difference between the "reduced" cross sections is found to be even larger, see Fig.6 of Ref. [1]. The experimentalists have carried out a coupled channel (CC) analysis of the fusion data with phenomenological Woods-Saxon potentials which generally underpredict the data at low $E_{\rm c.m.}$ energies. In the case of ^{132}Sn+^{40}Ca, the CC model calculations yield cross sections which differ by a factor of 10 or more from the data, despite the fact that the optical model potentials contain 7 adjustable parameters. Interestingly, it is possible to get a good fit to the data using the empirical Wong model (tunneling through a single parabolic barrier, with 3 adjustable parameters). In this case the analysis reveals an unusually large curvature of the barrier, $\hbar\omega = 13.13 \pm 1.09$ MeV, for ^{132}Sn+^{40}Ca as compared to the ^{132}Sn+^{48}Ca system with only $\hbar\omega = 5.77 \pm 0.52$ MeV. A large curvature implies a narrow parabolic barrier. Of course, these values are simply fits to the measured data; the model does not explain why the barrier curvatures are so dramatically different. As we will see, our microscopic DC-TDHF theory describes these results naturally in terms of the underlying mean-field dynamics, without any adjustable parameters.

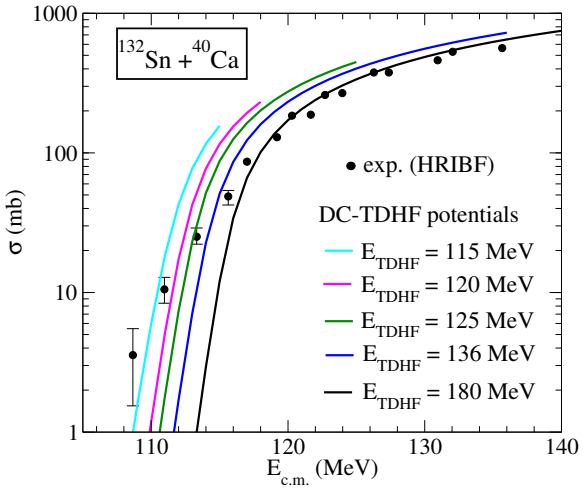

FIG. 4. (Color online) Total fusion cross sections for ^{132}Sn+^{40}Ca. The cross sections have been calculated with the DC-TDHF method for several energy-dependent ion-ion potentials $U(\bar{R})$ some of which are displayed in Fig. 3. The experimental data are taken from Ref. [1].

In Fig. 4 we show the excitation function of the total fusion cross section for ^{132}Sn+^{40}Ca. The cross sections have been calculated with five different energy-dependent ion-ion potentials; the corresponding DC-TDHF energies are listed in the figure. The main point of the chosen display is to demonstrate that the energy-dependence of the heavy-ion potential is crucial for an understanding of the strong fusion enhancement at subbarrier energies: At very high energy ($E_{\rm TDHF} = 180$ MeV) the potential approaches the limit of the frozen density approximation: the collision is so fast that the nuclei have no time to rearrange their densities. We observe that the measured fusion cross sections at energies $E_{\rm c.m.} > 118$ MeV are well-described by this high-energy potential.

As we have seen in Fig. 3, the potential barrier height decreases dramatically as we lower the energy $E_{\rm TDHF}$. Due to the slow motion of the nuclei at sub-barrier energies, the nuclear densities have time to rearrange resulting in neck formation, neutron transfer, and surface vibrations. All of these effects are included in DC-TDHF, and apparently they reduce the fusion barrier height and strongly modify the interior region of the heavy-ion interaction potential. As a result of the decrease in the fusion barrier, one finds strongly enhanced fusion cross sections at low sub-barrier energies. In particular, we observe that the data points measured at the two lowest energies $E_{\rm c.m.} = 108.6$ and 111 MeV are described well by the heavy-ion potential calculated at $E_{\rm TDHF} = 115$ MeV. This is the lowest-energy potential $U(\bar{R})$ we have been able to calculate using the DC-TDHF method, with a potential barrier $E_B = 111.5$ MeV located at $\bar{R} = 12.4$ fm.

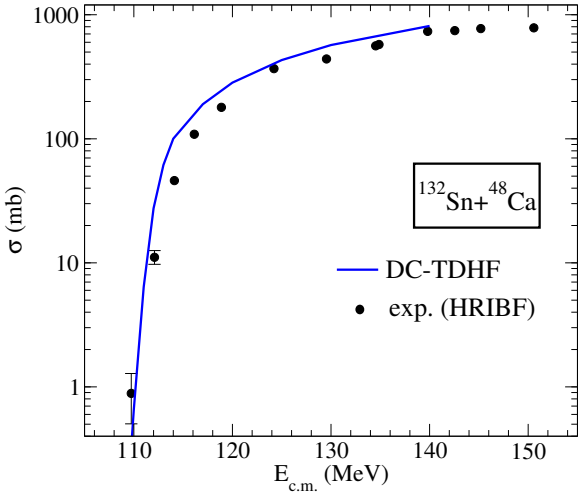

FIG. 5. (Color online) Total fusion cross section obtained with the DC-TDHF method for ^{132}Sn+^{48}Ca. Cross sections calculated for several energy-dependent ion-ion potentials [26] have been interpolated in this case (single blue line). The experimental data are taken from Ref. [1].

In Fig. 5 we show total fusion cross sections for ^{132}Sn+^{48}Ca which contains 8 additional neutrons. In this case, we have interpolated the theoretical cross sections obtained with the energy-dependent DC-TDHF potentials [26]. We can see that our theoretical cross sections

agree remarkably well with the experimental data. The main experimental puzzle, i.e. the fact that the low-energy sub-barrier fusion cross section for ^{132}Sn+^{40}Ca is substantially enhanced as compared to the more neutron-rich system ^{132}Sn+^{48}Ca, can be understood by examining the transformed ion-ion potential shown in Fig. 2. Both systems are found to have approximately the same barrier heights and positions, but the barrier for ^{40}Ca has a *narrower width*, resulting in enhanced fusion. Our DC-TDHF approach naturally explains the results of the experimental data analysis which used the empirical Wong model fit (see remarks at the beginning of this section). However, the microscopic potential barrier is not a simple parabola, and the DC-TDHF ion-ion potential is found to depend strongly on the energy $E_{\rm c.m.}$ for heavy systems.

Is there a correlation between fusion enhancement and neutron transfer? In Ref. [28], a quantum diffusion approach was used to explain the sub-barrier enhancement for ^{40}Ca in terms of neutron transfer leading to a dynamical onset of deformations. However, in microscopic theories like TDHF it is difficult to isolate individual effects that lead to the modification of the inner barrier region. Generally, the inner part of the barrier is determined by the dynamics of the neck. In this sense transfer does influence the inner part of the barrier. According to Ref. [1], the Q-values for neutron pickup by ^{40}Ca in the reaction ^{132}Sn+^{40}Ca are positive. Similarly, one finds positive Q-values for proton stripping and for combined neutron pickup plus proton stripping. By contrast, the corresponding Q-values are negative for the ^{132}Sn+^{48}Ca reaction. Based on these Q-values, one would expect enhanced neutron pickup and proton stripping for ^{40}Ca in comparison to ^{48}Ca. In order to elucidate the role of transfer in TDHF, we have computed the change in the neutron and proton numbers associated with the two calcium isotopes as a function of the internuclear distance R. The results are shown in Fig. 6. As expected from the Q-values, our TDHF calculations show a substantial increase in proton stripping from ^{40}Ca (dashed red line) as compared to ^{48}Ca (solid red line). This can also be understood by the fact that the protons in ^{48}Ca are more strongly bound than in ^{40}Ca. By contrast, we find that the neutron pickup by ^{40}Ca (dashed blue line) is fairly similar to that found for ^{48}Ca (solid blue line). This somewhat surprising result might suggest that Q-values alone cannot explain the detailed structure of multi-nucleon transfer in these fusion reactions.

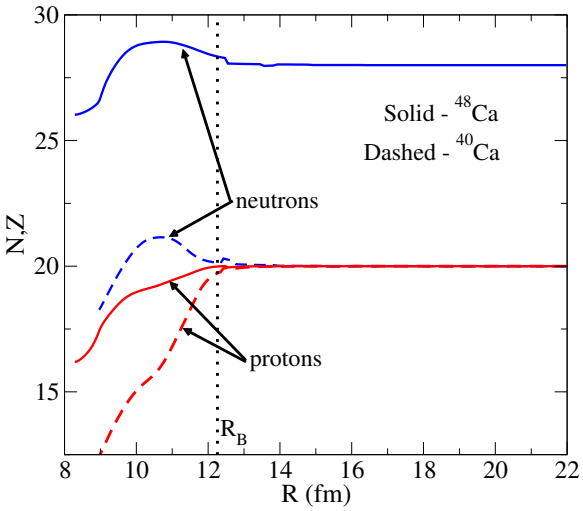

FIG. 6. (Color online) Neutron transfer (blue) and proton transfer (red) as a function of the internuclear distance R for the fusion reactions ^{132}Sn+^{40,48}Ca at $E_{\rm c.m.}$ = 120 MeV and impact parameter b = 0. Solid lines are for ^{48}Ca and dashed lines are for ^{40}Ca. The potential barrier is located at R_B = 12.3 fm.

IV. SUMMARY

In this paper, we calculate heavy-ion interaction potentials and total fusion cross sections for ^{132}Sn+^{40}Ca at energies $E_{\rm c.m.}$ below and above the Coulomb barrier, and we compare these results to the more neutron-rich system ^{132}Sn+^{48}Ca studied earlier [26]. The ion-ion potential calculations are carried out utilizing a dynamic microscopic approach, the Density Constrained Time-Dependent Hartree-Fock (DC-TDHF) method. The single-particle wave functions are generated on a 3D Cartesian lattice which spans 50 fm along the collision axis and 30 − 42 fm in the other two directions. The only input is the Skyrme N-N interaction, there are no adjustable parameters.

The main objective of this paper is to give a theoretical analysis of fusion cross sections which were measured recently at HRIBF. The experimental data show a surprising enhancement at low $E_{\rm c.m.}$ energies for the system ^{132}Sn+^{40}Ca as compared to the more neutron-rich system ^{132}Sn+^{48}Ca. Based on geometric considerations, one would expect the opposite: as a result of the increased nuclear radius for ^{48}Ca, the fusion barrier for ^{132}Sn+^{48}Ca should be reduced which in turn should increase the fusion cross section. Using the microscopic DC-TDHF approach we are able to explain the measured sub-barrier fusion enhancement in terms of the *narrower width* of the ion-ion potential for ^{132}Sn+^{40}Ca, while the barrier heights and positions are approximately the same in both systems.

While for the fusion of light nuclei the microscopic ion-ion potentials are almost independent of the *c.m.* energy, for heavier systems a strong energy-dependence is observed. With increasing *c.m.* energy, the height of the potential barrier increases, and the barrier peak moves inward towards smaller internuclear distances (see Fig. 3). This behavior of the ion-ion potential has a dramatic influence on the sub-barrier fusion cross sections. For the system ^{132}Sn+^{40}Ca, we have calculated heavy-ion interaction potentials at 8 different energies ranging from $E_{\rm TDHF}$ = 115 MeV to $E_{\rm TDHF}$ = 180 MeV. The time-dependent and density constraint calculations are com-

putationally very intensive. The total CPU time in this case amounts to 192 days on a single Intel Xeon processor. Our calculations are performed on a Dell LINUX workstation with 12 processors using OpenMP, which reduces this time to about 16 days.

ACKNOWLEDGMENTS

This work has been supported by the U.S. Department of Energy under Grant No. DE-FG02-96ER40975 with Vanderbilt University.

[1] J. J. Kolata, A. Roberts, A. M. Howard, D. Shapira, J. F. Liang, C. J. Gross, R. L. Varner, Z. Kohley, A. N. Villano, H. Amro, W. Loveland, and E. Chavez, Phys. Rev. C **85**, 054603 (2012).
[2] J. W. Negele, Rev. Mod. Phys. **54**, 913 (1982).
[3] C. Simenel, Phys. Rev. Lett. **106**, 112502 (2011).
[4] A. S. Umar, M. R. Strayer, J.-S. Wu, D. J. Dean, and M. C. Güçlü, Phys. Rev. C **44**, 2512 (1991).
[5] A. S. Umar and V. E. Oberacker, Phys. Rev. C **73**, 054607 (2006).
[6] C. Simenel, Eur. Phys. J. A **48:** 152 (2012).
[7] Lu Guo, J. A. Maruhn, P.-G. Reinhard, and Y. Hashimoto, Phys. Rev. C **77**, 041301(R) (2008).
[8] Kouhei Washiyama and Denis Lacroix, Phys. Rev. C **78**, 024610 (2008).
[9] E. Chabanat, P. Bonche, P. Haensel, J. Meyer and R. Schaeffer, Nucl. Phys. **A635**, 231 (1998); **A643**, 441(E) (1998).
[10] P. Klüpfel, P.-G. Reinhard, T. J. Bürvenich, and J. A. Maruhn, Phys. Rev. C **79**, 034310 (2009).
[11] M. Kortelainen, T. Lesinski, J. Moré, W. Nazarewicz, J. Sarich, N. Schunck, M. V. Stoitsov, and S. Wild, Phys. Rev. C **82**, 024313 (2010).
[12] A. S. Umar, M. R. Strayer, and P.-G. Reinhard, Phys. Rev. Lett. **56**, 2793 (1986).
[13] A. S. Umar and V. E. Oberacker, Phys. Rev. C **74**, 021601(R) (2006).
[14] V. E. Oberacker, A. S. Umar, J. A. Maruhn, and P.-G. Reinhard, Phys. Rev. C **82**, 034603 (2010).
[15] A. S. Umar and V. E. Oberacker, Phys. Rev. C **74**, 061601(R) (2006).
[16] A. S. Umar and V. E. Oberacker, Phys. Rev. C **76**, 014614 (2007).
[17] A. S. Umar and V. E. Oberacker, Eur. Phys. J. A **39**, 243 (2009).
[18] A. S. Umar, V. E. Oberacker, J. A. Maruhn, and P.-G. Reinhard, Phys. Rev. C **81**, 064607 (2010).
[19] R. Keser, A. S. Umar, and V. E. Oberacker, Phys. Rev. C **85** 044606 (2012).
[20] A. S. Umar, V. E. Oberacker, and C. J. Horowitz, Phys. Rev. C **85** 055801 (2012).
[21] K. Hagino and Y. Watanabe, Phys. Rev. C **76**, 021601(R) (2007).
[22] M. Dasgupta, D. J. Hinde, A. Diaz-Torres, B. Bouriquet, Catherine I. Low, G. J. Milburn, and J. O. Newton, Phys. Rev. Lett. **99**, 192701 (2007).
[23] Takatoshi Ichikawa, Kouichi Hagino, and Akira Iwamoto, Phys. Rev. Lett. **103**, 202701 (2009).
[24] H. Esbensen, C. L. Jiang, and A. M. Stefanini, Phys. Rev. C **82**, 054621 (2010).
[25] A. S. Umar and V. E. Oberacker, Phys. Rev. C **77**, 064605 (2008).
[26] V. E. Oberacker, A. S. Umar, J. A. Maruhn, and P.-G. Reinhard, Phys. Rev. C **85**, 034609 (2012).
[27] A. S. Umar, V. E. Oberacker, J. A. Maruhn, and P.-G. Reinhard, Phys. Rev. C **80**, 041601(R) (2009).
[28] V. V. Sargsyan, G. G. Adamian, N. V. Antonenko, W. Scheid, and H. Q. Zhang, Phys. Rev. C **85**, 024616 (2012).